Mechanically Induced Metal Insulator Transition in Carbyne

ARTICLE *in* NANO LETTERS · FEBRUARY 2013

Impact Factor: 13.59 · DOI: 10.1021/nl5017317 · Source: arXiv

3 AUTHORS, INCLUDING:

Vasilii Artyukhov
Rice University
31 PUBLICATIONS **435** CITATIONS
SEE PROFILE

Mingjie Liu
Rice University
10 PUBLICATIONS **146** CITATIONS
SEE PROFILE

Mechanically induced metal–insulator transition in carbyne

Vasilii I. Artyukhov and Mingjie Liu
Department of Mechanical Engineering and Materials Science, Rice University, Houston, Texas 77005

Boris I. Yakobson
Department of Mechanical Engineering and Materials Science, Department of Chemistry and Smalley Institute for Nanoscale Science and Technology, Rice University, Houston, Texas 77005, USA *

First-principles calculations for carbyne under strain predict that the Peierls transition from symmetric cumulene to broken-symmetry polyyne structure is enhanced as the material is stretched. Interpretation within a simple and instructive analytical model suggests that this behavior is valid for arbitrary 1D metals. Further, numerical calculations of the anharmonic quantum vibrational structure of carbyne show that zero-point atomic vibrations alone eliminate the Peierls distortion in a mechanically free chain, preserving the cumulene symmetry. The emergence and increase of Peierls dimerization under tension then implies a qualitative transition between the two forms, which our computations place around 3% strain. Thus, zero-point vibrations and mechanical strain jointly produce a change in symmetry resulting in the transition from metallic to insulating state. In any practical realization, it is important that the effect is also chemically modulated by the choice of terminating groups. Our findings are promising for applications such as electromechanical switching and band gap tuning via strain, and besides carbyne itself, they directly extend to numerous other systems that show Peierls distortion.

Carbyne—the linear allotrope of carbon—is perhaps one of the most unusual materials due to its ultimate one-atom thinness. Although carbyne is elusively hard to prepare and has been perceived as an exotic or even completely fictitious material, the development of methods to synthesize carbon chains proceeds at a steady rate, with input from both experiments and theory.[1–7] Among the most notable recent achievements, chains with length of up to 44 atoms[8] and such complex molecular machines as carbyne-based rotaxanes[9,10] have been synthesized. This progress is driven by carbyne's attractive physical properties such as unusual electrical transport[11,12] and intriguing mechanics,[13] or its large specific area.[14] Accordingly, a better theoretical understanding of this material is becoming more and more relevant.[13]

It has long ago been established by the quantum chemistry community[15] that carbyne undergoes the Peierls transition[16–19] that converts it from the cumulene $(=C=C=)_n$ to the polyyne $(-C\equiv C-)_n$ form. Later it has been suggested that the zero-point vibrations (ZPV) may substantially affect the Peierls instability[20] and even completely eliminate the distortion in carbyne.[21] As the symmetric and broken-symmetry forms have very distinct electronic properties (metallic and insulating, respectively), this issue becomes crucial from both the fundamental physicochemical perspective and for applications in 1D conducting systems.

A whole new dimension is added to the situation by the unusual effects of stretching on carbyne that we have recently found through first-principles calculations[13] (also observed experimentally after the present study had been completed.[22]) Specifically, stretching increases the bond length alternation (BLA, defined as the difference between the long and short bonds) and the band gap. Although the effect of strain on the band gap is well-known in semiconductors, the present case is very abnormal—see discussion in Supplementary Information (SI)—both in the sign of the dependence and the greater amplitude ($\partial Eg/\partial\epsilon$ = 12.3–29.7 eV, see Fig. 1), indicating a different nature of the effect.

Thus, we start with an exploration of the effect of strain on the Peierls transition. We use a simple analytical model to explain why tension amplifies the Peierls effect. Then we investigate through first-principles Born–Oppenheimer potential energy surface calculations how the atomic vibrations manifest themselves in equilibrium and under strain. We confirm that the ZPV level lies well above the Peierls transition energy, and the instability is eliminated. As this energy is increased by tension, we arrive at the prediction of a strain threshold whereupon carbyne switches from the ZPV– to Peierls instability–dominated regime, accompanied by a sharp change in the electrical conductivity. Our first-principles numerical analysis validates this prediction, placing this transition around 3% strain. Besides carbyne, our findings naturally suggest that this novel physical effect must also be observable in other one-dimensional systems exhibiting Peierls behavior, such as conducting polymers, charge-density-wave materials, or carbon nanotubes.[23]

Our first-principles data on the amplification of the Peierls instability under tension are presented in **Fig. 1**. The Peierls distortion is extremely sensitive to the electronic exchange interaction and, in particular, is poorly described by regular density functional theory,[24] therefore we used the HSE06 hybrid functional that includes exact exchange.[25,26] All calculations were also repeated with the PBE generalized-gradient functional,[27,28] showing complete qualitative agreement (see SI). Circles and squares represent the BLA (left axis) and the band gap E_g (right axis). The Peierls transition energy

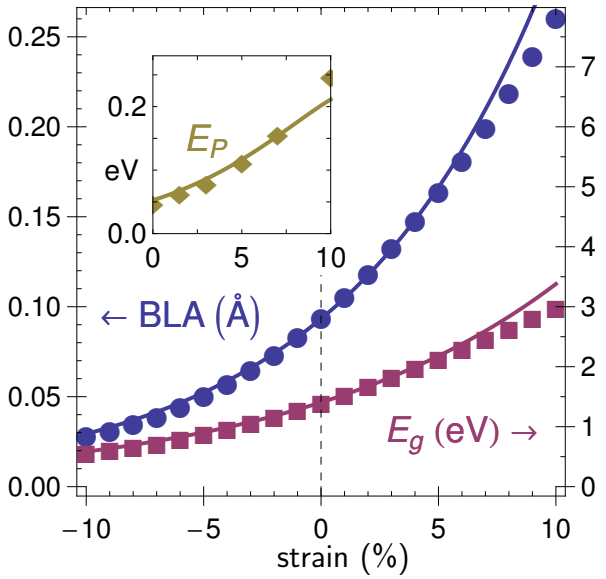

FIG. 1: **Bond length alternation (BLA), band gap (E_g), and Peierls barrier (E_P, inset) as a function of strain.** Points, DFT calculation results. Lines, fitting based on the analytical model. The fitting is performed in the [–5%, 5%] strain range assuming that the lattice stiffness decreases linearly with strain, and is done independently for BLA and E_g. The E_P line in the inset is computed based on the BLA fit.

E_P—energy difference between polyyne and cumulene structures—is shown in the inset. The striking increase of all quantities observed so pronouncedly in **Fig. 1** calls for an explanation.

One can understand the behavior of Peierls transition under strain using a simple and general model as follows. The lowering of electronic energy in the Peierls effect is $E_e \propto a|V_k|^2 \log|V_k|/k$, where k is the Brillouin zone edge ($k = \pi/a$) and V_k is the corresponding Fourier component of the lattice potential.[29] To determine $E_e(a)$, some definite form of the $V_k(a)$ dependence is needed. We use a simple Kronig–Penney type model with two delta-function atoms per period $2a$ with coordinates $x_1 = 0$ and $x_2 = (a-b)/2$, where b is the BLA (we assume $b > 0$). The potential in the unit cell is $V(x) = -\delta(x-x_1) - \delta(x-x_2)$, and then $|V_k| = 2|\sinh(\pi b/2a)| = \pi|b|/a + O\left(|b|^3/a^3\right)$. The electronic contribution is counteracted by the lattice deformation energy, $E_l = {}^1\!/_2 C b^2 + O\left(b^4\right)$. The value of b must minimize the total energy, $\partial(E_e+E_l)/\partial b = -\pi b - \pi b \log\left(\pi\frac{b}{a}\right) + Cb = 0$, and we have the answer as $b = \frac{a}{\pi}\exp\left(-\frac{1}{2} - \frac{C}{2\pi}\right)$. The derivative db/da is positive when $2\pi - a\frac{dC}{da} > 0$, which shows that the Peierls dimerization is increased by tension unless the restoring force constant increases with strain (at least as fast as $C = C_0 + 2\pi\log a$—and usually the trend is opposite).

To demonstrate the excellent agreement of our very simple model with the DFT calculations, we have fitted it to our DFT data (**Fig. 1**). The fitting was done assuming simple linearly decreasing stiffness, $C \approx C_0 + D(a_0 - a)$, and used only the data points in the [–5%, 5%] strain interval. The fitting was performed independently for the BLA and E_g, and the former fit was used to compute the line for E_P.

Up until now, we have confined ourselves to the static picture of classical carbon atoms. Within this picture, only the polyyne form of carbyne is stable, and stretching it produces merely *quantitative* changes in the band gap—a phenomenon known in solid state physics, even though its origin here is unusual. However, as we demonstrate below, the quantized nuclear motion changes the picture dramatically. If ZPV can overpower the Peierls instability in freely-suspended unloaded chain and restore the symmetric metallic structure, then one is led to expect that at some critical strain, the stronger Peierls instability may reverse this phenomenon—causing a *qualitative* change in properties. Our calculations indeed confirm this.

For the vibrational analysis we computed the Born–Oppenheimer potential energy surface (PES) profiles along the BLA coordinate, $E_a(b)$, as the lattice constant a was increased from its equilibrium value. Because of the extreme anharmonicity of the ω-shaped PES profiles, we had to turn to numerical calculations of the vibrational levels at each strain value. We utilized the Fourier grid Hamiltonian method[30,31] which had been previously used to study the ZPV effect on Peierls transition in unstrained polyacetylene.[32] Following Refs.[21,32] we assume that the longitudinal vibrations can be decoupled from the two transverse phonons and treated in isolation, which is justified by the non-negligible bending stiffness of carbyne.[33–35] (Indeed, the inclusion of transverse vibrations and dispersion does not change our conclusions, as detailed in the SI.) We used a uniform grid of 250 points in -0.4 Å $\le b \le 0.4$ Å, using interpolation of DFT-computed values of energy, and 6.005 a.m.u.—the reduced mass of two C atoms—for the oscillator mass.

The results are presented in **Fig. 2**, which is the central figure of this paper. The black curves show the ω-shaped PES as computed using the HSE06 functional, blue horizontal lines denote the computed vibrational levels with filling below the zero level, and the red-to-blue curves plot the ZPV wavefunction. The right panels show reconstructed real-space densities of nuclei at the respective strain values. The profile along the horizontal axis is the squared vibrational wavefunctions with an arbitrary transverse broadening. Colors represent which values of BLA (positive or negative in the left-hand side plots) correspond to the position.

Clearly, the mechanically relaxed system has a single wavefunction maximum with a width exceeding the BLA,[20] corresponding to the cumulene structure of carbyne with lattice parameter $a/2$. Thus, ZPV stabilize the cumulene form even though it is a maximum on the PES. In accordance with the above discussion, the central PES maximum (E_P) rises with strain, and at 3%, the wavefunction develops a slight dip in the center, resulting in a

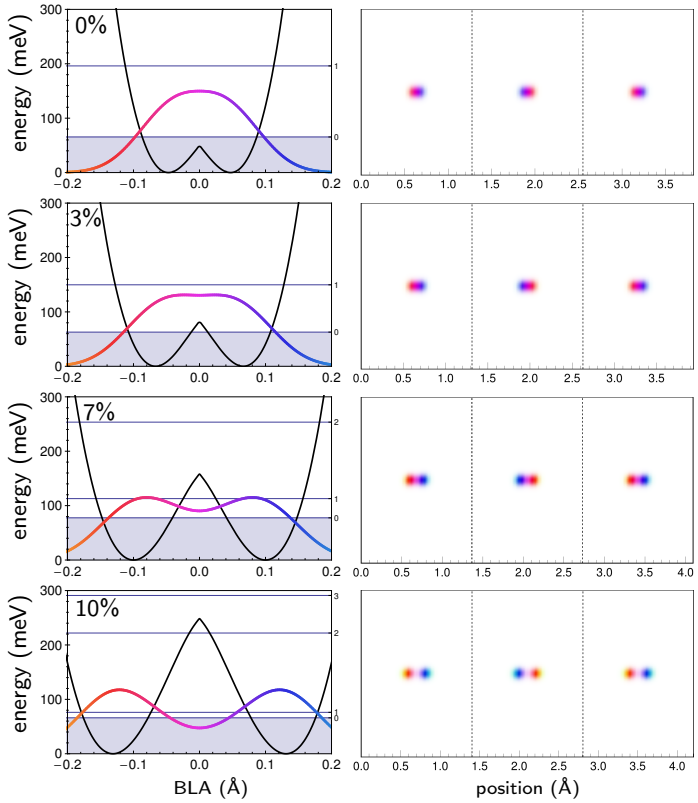

FIG. 2: **Zero-point vibrations under strain. (left)** Evolution of the vibrational structure of carbyne with strain. The ω-shaped lines show the **potential energy** as a function of BLA. Horizontal lines show the vibrational levels, the shaded region is below the **ZPV level**. **(right)** Real-space atomic density distributions based on ZPV wavefunctions (three one-atom unit cells shown, color indicates which part of the BLA wavefunction the density comes from).

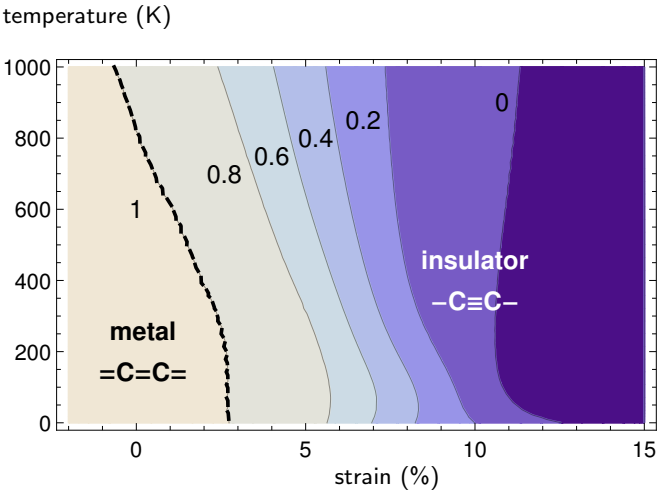

FIG. 3: **Strain–temperature "phase diagram" of the polyyne–cumulene transition.** The order parameter R (see the text) measures the shape of the nuclear density distribution, with one maximum (cumulene) at $R = 1$ and two (polyyne) at $R < 1$.

picture of 'elongated' atoms. At 7% strain, the ground-state wavefunction is clearly separated in two blobs, and the first excited level approaches the ground state, indicative of the transition to the double-well potential–like regime. Under further stretching (10%), the first excited level is well below room-temperature k_BT of the ground state, as in two independent potential wells. The second level dives below the Peierls barrier, and the third begins to approach it (at 15% strain these two also become degenerate; data not shown). The joint evolution of Peierls barrier and vibrational levels under stretching is further illustrated in the SI (Fig. S2).

The above-described sequence of events has a profound consequence. As the strain is increased, carbyne transitions from the conducting electronic behavior of cumulene to the nonconductive polyyne structure with its sizable band gap (see **Fig. 1**). One can go a step further and compute a strain–temperature "phase diagram" for carbyne. First, the temperature-dependent nuclear densities $n_T(b)$ are computed using Bose statistics from squared wavefunctions. A rising temperature and strain-induced depression of vibrational levels start to populate the first excited states which have small amplitude near $b = 0$, and $n_T(b)$ becomes wider until its central maximum splits in two. To determine the polyynic or cumulenic character, for the role of order parameter we used a measure of the distribution shape: the ratio $R = n_T(0) / \max_b(n_T(b))$, which is 1 always when there is a single central minimum (pure cumulene) and less than 1 when the symmetry is broken. **Fig. 3** shows a contour map of R. The region to the left of the $R = 1$ contour corresponds to pure cumulene. At low temperatures, the threshold strain is 3% and it decreases with temperature starting from about 200 K, until at 900 K, the cumulene form becomes unstable (unless compressed, which is hard to picture with carbyne but may be feasible for other systems such as carbon nanotubes). Note that in the canonical Peierls effect, high temperatures tend to restore symmetry. That is an electronic excitation effect, and it should be negligible given polyyne's wide band gap. (Further, this effect could only result in a shift of the transition to larger strains.) Thus, once again we see that the inclusion of nuclear degrees of freedom in the picture has led to unexpected qualitative changes of behavior.

Besides the strain and temperature, the composition of carbyne provides offers another degree of freedom. With ^{13}C instead of ^{12}C, all levels would experience a slight red-shift, moving the cumulene stability boundary closer to the origin. Formally, lighter C isotopes (had such existed) or lighter elements (assuming constant bond stiffness) would have moved the boundary up and to the right.

So far our calculations treated carbyne as an infinite chain. The PES of infinite carbyne contains pairs of minima and is invariant under translation by one-half the

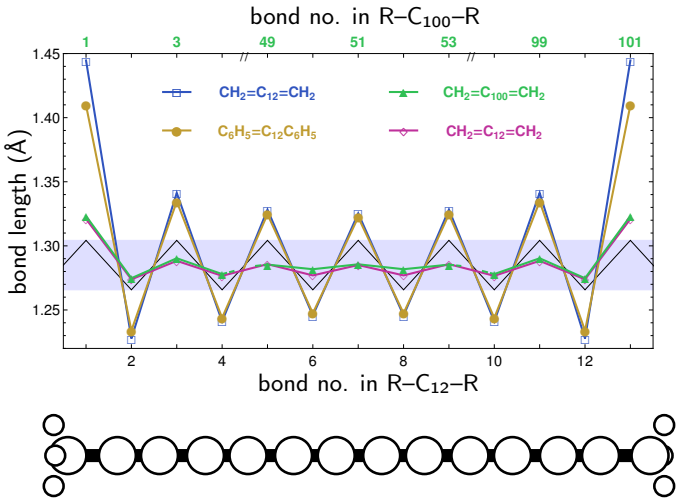

FIG. 4: **Effect of endgroups on carbyne BLA.** Termination of the chain with sp^3 groups (methyl **–CH$_3$** and phenyl **–C$_6$H$_5$**) increases the BLA, whereas the sp^2 methylene group (**=CH$_2$**) decreases it, as compared to an unterminated infinite chain (black dashed line). The data for **12-** and **100-atom** chains show a weak decrease of BLA with chain length away from the ends with methylene termination.

unit cell of polyyne, which corresponds to the exchange of triple and single bonds. However, the ends of the carbyne chain, inevitable in any real experiment, will impose some boundary conditions that can break this degeneracy. (Note that our predictions should still apply directly to carbyne rings.) As a simple example, the two *finite* structures described by structural formulae

$$\mathrm{H-C\left(\equiv C-C\equiv\right)}_n\mathrm{C-H}$$

and

$$\mathrm{H\equiv C\left(-C\equiv C-\right)}_n\mathrm{C\equiv H}$$

are very nondegenerate, because H cannot even form stable triple bonds with C. On the other hand, the use of groups that interface with the chain through a double bond, such as methylene =CH$_2$, could favor the cumulene structure and stabilize the symmetry. The effect of end-groups will clearly have a different strength for different moieties, and a comprehensive investigation is an extensive task (further aggravated by the complexity of collective atomic motions in such many-atom systems) that is beyond the scope of the present study. However, simply looking at how the BLA depends on the end-group type in finite carbyne fragments already provides a useful glance into the issue.

The results of our finite-chain calculations with different terminating groups are presented in **Fig. 4**. The strip from 1.27 to 1.30 Å denotes the bond lengths in the ideal infinite polyyne chain (ignoring the ZPV). The bond lengths in the sp^3-terminated systems (–CH$_3$, –C$_6$H$_5$) fall outside this strip, showing the enhanced polyyne-like character of the systems. On the other hand, sp^2-type =CH$_2$ termination reduces the BLA effectively to zero (< 0.01 Å for a 12-atom chain and < 0.005 Å in the middle of a 100-atom chain), suggesting that this type of passivation may even be used to shift the transition boundary towards higher strains/temperatures. (Indeed, sp^2-type groups are preferable from the electronics applications standpoint, providing metallic 'leads' at the ends of the chain.) We see that in experimental realizations, the switching effect may be destroyed by improper chemical termination of carbyne chains, and thus, precise control over both the tension and chemistry is essential.

In conclusion, we have explored how the Peierls instability of linear carbon chains is enhanced by stretching using first-principles calculations, and explained it with a simple analytical model. At zero strain, the Peierls instability in carbyne is too weak compared to quantum zero-point vibrations, and the stable structure corresponds to the metallic cumulene rather than insulating polyyne—despite the lower potential energy of the latter structure. However, the enhancement of Peierls instability results in the reversal of this effect, and carbyne starts to demonstrate the polyyne-like character of the nuclear wavefunction, switching from the conducting to insulating behavior around 3% strain. This effect naturally applies to other one-dimensional Peierls systems. Our findings are both important as an interesting new fundamental physical effect and highly practically relevant for the science of conducting polymers, charge- and spin-density-wave materials, and electromechanical applications. Although carbyne remains an exotic, its unique properties will continue to fuel the effort to achieve its synthesis in practically useful quantities.

The computations were performed using the VASP code[36] with projector-augmented wave basis sets,[37,38] using the Data Analysis and Visualization Cyberinfrastructure funded by NSF under Grant OCI-0959097.

* Electronic address: biy@rice.edu

[1] Cataldo, F. (ed.) *Polyynes: synthesis, properties, and applications* (CRC Press, Boca Raton, 2005).
[2] Jin, C., Lan, H., Peng, L., Suenaga, K. & Iijima, S. Deriving carbon atomic chains from graphene. *Phys. Rev. Lett.* **102**, 205501 (2009).
[3] Hobi, E., Pontes, R. B., Fazzio, A. & da Silva, A. J. R. Formation of atomic carbon chains from graphene nanoribbons. *Phys. Rev. B* **81**, 201406 (2010).
[4] Erdogan, E. *et al.* Engineering carbon chains from mechanically stretched graphene-based materials. *Phys. Rev. B* **83**, 041401 (2011).
[5] Casillas, G. *et al.* New insights into the properties and interactions of carbynes as revealed by HRTEM and DFT

analysis (2013). (submitted).

[6] Yakobson, B., Campbell, M., Brabec, C. & Bernholc, J. High strain rate fracture and c-chain unraveling in carbon nanotubes. *Comp. Mater. Sci.* **8**, 341–348 (1997).

[7] Troiani, H. E. *et al.* Direct observation of the mechanical properties of single-walled carbon nanotubes and their junctions at the atomic level. *Nano Lett.* **3**, 751–755 (2003).

[8] Chalifoux, W. & Tykwinski, R. Synthesis of polyynes to model the sp-carbon allotrope carbyne. *Nature Chem.* **2**, 967–971 (2010).

[9] Movsisyan, L. D. *et al.* Synthesis of polyyne rotaxanes. *Org. Lett.* **14**, 3424—3426 (2012).

[10] Weisbach, N., Baranová, Z., Gauthier, S., Reibenspies, J. H. & Gladysz, J. A. A new type of insulated molecular wire: a rotaxane derived from a metal-capped conjugated tetrayne. *Chem. Commun.* **48**, 7562—7564 (2012).

[11] Khoo, K. H., Neaton, J. B., Son, Y. W., Cohen, M. L. & Louie, S. G. Negative differential resistance in carbon atomic wire-carbon nanotube junctions. *Nano Lett.* **8**, 2900–2905 (2008).

[12] Zanolli, Z., Onida, G. & Charlier, J.-C. Quantum spin transport in carbon chains. *ACS Nano* **4**, 5174–5180 (2010).

[13] Liu, M., Lee, H. & Yakobson, B. I. Carbynes by the first principles computations: an ultimate 1D-Material. IMECE2012–89610 (Houston, TX, USA, 2012). URL `http://www.asmeconferences.org/congress2012/`.

[14] Sorokin, P. B., Lee, H., Antipina, L. Y., Singh, A. K. & Yakobson, B. I. Calcium-decorated carbyne networks as hydrogen storage media. *Nano Lett.* **11**, 2660–2665 (2011).

[15] Kertesz, M., Koller, J. & Azman, A. Ab initio Hartree–Fock crystal orbital studies. II. energy bands of an infinite carbon chain. *J. Chem. Phys.* **68**, 2779–2782 (1978).

[16] Peierls, R. E. Zur Theorie der elektrischen und thermishen Leftfähigkeit von Metallen. *Ann. Phys. (Leipzig)* **4**, 121–148 (1930).

[17] Peierls, R. E. *Quantum Theory of Solids* (Clarendon Press, Oxford, 2001).

[18] Fröhlich, H. On the theory of superconductivity: The one-dimensional case. *Proc. R. Soc. Lond. A* **223**, 296–305 (1954).

[19] Kennedy, T. & Lieb, E. H. Proof of the Peierls instability in one dimension. *Phys. Rev. Lett.* **59**, 1309–1312 (1987).

[20] McKenzie, R. H. & Wilkins, J. W. Effect of lattice zero-point motion on electronic properties of the Peierls-Fröhlich state. *Phys. Rev. Lett.* **69**, 1085–1088 (1992).

[21] Tongay, S., Dag, S., Durgun, E., Senger, R. T. & Ciraci, S. Atomic and electronic structure of carbon strings. *J. Phys.: Condens. Matter* **17**, 3823–3836 (2005).

[22] Cretu, O. *et al.* Electrical conductivity measured in atomic carbon chains. *arXiv:1302.5207* (2013).

[23] Mintmire, J. W., Dunlap, B. I. & White, C. T. Are fullerene tubules metallic? *Phys. Rev. Lett.* **68**, 631–634 (1992).

[24] Jacquemin, D. *et al.* Assessment of several hybrid DFT functionals for the evaluation of bond length alternation of increasingly long oligomers. *J. Phys. Chem. A* **110**, 5952–5959 (2006).

[25] Heyd, J., Scuseria, G. E. & Ernzerhof, M. Hybrid functionals based on a screened coulomb potential. *J. Chem. Phys.* **118**, 8207–8215 (2003).

[26] Heyd, J., Scuseria, G. E. & Ernzerhof, M. Erratum: "Hybrid functionals based on a screened coulomb potential". *J. Chem. Phys.* **124**, 219906 (2006).

[27] Perdew, J. P., Burke, K. & Ernzerhof, M. Generalized gradient approximation made simple. *Phys. Rev. Lett.* **77**, 3865–3868 (1996).

[28] Perdew, J. P., Burke, K. & Ernzerhof, M. Generalized gradient approximation made simple [phys. rev. lett. 77, 3865 (1996)]. *Phys. Rev. Lett.* **78**, 1396 (1997).

[29] Mihály, L. & Martin, M. C. *Solid State Physics: Problems and Solutions* (John Wiley & Sons, New York, 2009).

[30] Marston, C. C. & Balint-Kurti, G. G. The fourier grid hamiltonian method for bound state eigenvalues and eigenfunctions. *J. Chem. Phys.* **91**, 3571–3576 (1989).

[31] Johnson III, R. D. Fourier grid hamiltonian 1D program. URL `http://www.nist.gov/mml/chemical_properties/computational/fourier_grid_hamiltonian.cfm`.

[32] Hudson, B. S. & Allis, D. G. Bond alternation in infinite periodic polyacetylene: Dynamical treatment of the anharmonic potential. *J. Mol. Struct.* **1032**, 78–82 (2013).

[33] Ravagnan, L. *et al.* Effect of axial torsion on sp carbon atomic wires. *Phys. Rev. Lett.* **102**, 245502 (2009).

[34] Hu, Y. H. Bending effect of sp-hybridized carbon (carbyne) chains on their structures and properties. *J. Phys. Chem. C* **115**, 1843–1850 (2011).

[35] Castelli, I. E., Salvestrini, P. & Manini, N. Mechanical properties of carbynes investigated by ab initio total-energy calculations. *Phys. Rev. B* **85**, 214110 (2012).

[36] Kresse, G. & Furthmüller, J. Efficient iterative schemes for ab initio total-energy calculations using a plane-wave basis set. *Phys. Rev. B* **54**, 11169—11186 (1996).

[37] Blöchl, P. E. Projector augmented-wave method. *Phys. Rev. B* **50**, 17953 (1994).

[38] Kresse, G. & Joubert, D. From ultrasoft pseudopotentials to the projector augmented-wave method. *Phys. Rev. B* **59**, 1758–1775 (1999).